A New Quick-Response and High-Efficiency Control Strategy of an Induction Motor

ISAO TAKAHASHI, MEMBER, IEEE, AND TOSHIHIKO NOGUCHI

Abstract—**New quick-response and high-efficiency control of an induction motor, which is quite different from that of the field-oriented control is proposed. The most obvious differences between the two are as follows. 1) The proposed scheme is based on limit cycle control of both flux and torque using optimum PWM output voltage; a switching table is employed for selecting the optimum inverter output voltage vectors so as to attain as fast a torque response, as low an inverter switching frequency, and as low harmonic losses as possible. 2) The efficiency optimization in the steady-state operation is also considered; it can be achieved by controlling the amplitude of the flux in accordance with the torque command. To verify the feasibility of this scheme, experimentation, simulation, and comparison with field-oriented control are carried out. The results prove the excellent characteristics for torque response and efficiency, which confirm the validity of this control scheme.**

I. Introduction

ACCORDING to the advance of factory automation, servo systems became indispensable to applications such as industrial robots and numerically controlled machinery. Especially the progress of an ac-servo system is remarkable, owing to the fact that it is maintenance-free. In recent years, field-oriented control has been employed that enables an induction motor to attain as quick torque response as a dc motor. The principle of its torque generation is based on the interaction between the flux and current, like a dc motor [1]. Fig. 1(a) is a system configuration of a typical field-orientation drive. In this system the flux current component I_0^* and the torque current component I_T^* are estimated from both flux command ψ_2^* and torque command T^* by using a calculator possessing motor parameters. The system usually employs a position sensor for coordinate transformation of the current components and a current-controlled inverter. Therefore, if the values used in the calculator deviate from the correct ones, both steady-state and transient response would be degraded. A number of papers have reported the problem and have explored the means of compensation [2]–[4]. There also remain some problems concerning instantaneous current control. Since the current-controlled inverter contains three independent hysteresis comparators, it is difficult to avoid increase of the inverter switching frequency, torque ripple, and harmonic losses of the machine in the steady-state operation. Moreover, when the PWM inverter saturates, sufficient torque response would not be expected.

Paper IPCSD 86-4, approved by the Industrial Drives Committee of the IEEE Industry Applications Society for presentation at the 1985 Industry Applications Society Annual Meeting, Toronto, ON, Canada, October 6–11. This work supported by the Heavy Apparatus Standard Products Department of the Toshiba Corporation. Manuscript released for publication February 5, 1986.

The authors are with the Technological University of Nagaoka, 1603-1 Kamitomioka, Nagaoka, Japan 949-54.

IEEE Log Number 8609012.

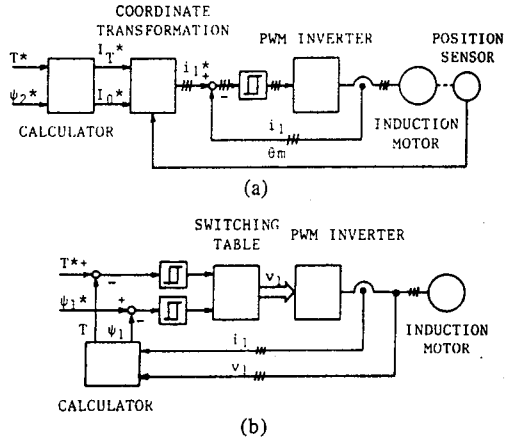

Fig. 1. Comparison of two schemes. (a) Field-oriented control. (b) New proposed scheme.

This paper describes a novel control scheme of an induction motor [5]. The principle of it is based on limit cycle control and it makes possible both quick torque response and high-efficiency operation at the same time. Fig. 1(b) shows the system configuration of the proposed scheme. In this system the instantaneous values of the flux and torque are calculated from only the primary variables. They can be controlled directly and independently by selecting optimum inverter switching modes. The selection is made so as to restrict the errors of the flux and torque within the hysteresis bands and to obtain the fastest torque response and highest efficiency at every instant. It enables both quick torque response in the transient operation and reduction of the harmonic losses and acoustic noise. Moreover, the implementation of an efficiency controller for the improvement of efficiency in the steady-state operation is also considered.

II. Dynamic Behavior of an Induction Motor

By using instantaneous vectors, the behavior of a machine can be conveniently expressed not only in the steady state but also in the transient state. In this section, to examine the transient torque response of an induction motor, an application of the vectors to the characteristic equations is described.

The primary voltage vector v_1 is defined by the following expression [6]:

$$v_1 = \sqrt{2/3}[v_{1a} + v_{1b} \exp(j2\pi/3) + v_{1c} \exp(j4\pi/3)] \quad (1)$$

where v_{1a}, v_{1b}, and v_{1c} are instantaneous values of the primary line-to-neutral voltages. Similarly, the primary current vector and the secondary current vector i_2 are given by

$$i_1=\sqrt{2/3}[i_{1a}+i_{1b}\ \exp\ (j2\pi/3)+i_{1c}\ \exp\ (j4\pi/3)] \quad (2)$$

$$i_2=\sqrt{2/3}[i_{2a}+i_{2b}\ \exp\ (j2\pi/3)+i_{2c}\ \exp\ (j4\pi/3)]. \quad (3)$$

These vectors are represented in a d-q stationary reference frame. Using the vector notation, the equations of a two-pole induction motor can be written as

$$\begin{bmatrix} v_1 \\ 0 \end{bmatrix} = \begin{bmatrix} R_1+pL_{11} & pM \\ (p-j\dot{\theta}_m)M & R_2+(p-j\dot{\theta}_m)L_{22} \end{bmatrix} \begin{bmatrix} i_1 \\ i_2 \end{bmatrix} \quad (4)$$

$$T=\psi_1 \cdot (-ji_1) \quad (5)$$

where

R_1 stator resistance,
R_2 rotor resistance,
L_{11} stator self-inductance,
L_{22} rotor self-inductance,
M mutual inductance,
$\dot{\theta}_m$ mechanical angular velocity,
T electromagnetic torque,
$\cdot$ scalar product,
ψ_1 primary flux linkage vector.

ψ_1 is given by

$$\psi_1=L_{11}i_1+Mi_2. \quad (6)$$

Under the condition of a constant amplitude of ψ_1, i.e., a constant amplitude of the magnetizing current vector i_0 of the stator, we will examine the torque step response of the motor. i_0 is obtained by dividing (6) by L_{11}:

$$i_0=\psi_1/L_{11}=i_1+(M/L_{11})i_2. \quad (7)$$

Both i_0 and i_1 can be written in the form of the polar coordinates as

$$i_0=I_0\ \exp\ (j\theta_0),\ i_1=I_1\ \exp\ (j\theta_0) \quad (8)$$

where I_0 is considered to be a constant reference vector and θ_0 is an angle between i_0 and the d-axis. Substituting (8) into (4) and (7), the following relation can be obtained from the rotor equation in (4):

$$I_1=\frac{R_2+(p+j\dot{\theta}_s)L_{22}}{R_2+(p+j\dot{\theta}_s)l}I_0 \quad (9)$$

where $l=(L_{11}L_{22}-M^2)/L_{11}$ and $\dot{\theta}_s=\dot{\theta}_0-\dot{\theta}_m$. $\dot{\theta}_s$ is an instantaneous slip angular frequency of ψ_1 referred to the rotor. Assuming the condition of constant $\dot{\theta}_m$, if the step change of $\dot{\theta}_0$ is applied at $t=0$, $\dot{\theta}_s$ can also be regarded to be stepwise at $t=0$ and then constant.

Substituting (7) and (8) into (5), the torque is represented by using I_0 and I_1.

$$T=L_{11}I_0\mathcal{L}^{-1}\ \{\mathrm{Im}\ I_1(s)\} \quad (10)$$

where $\mathcal{L}^{-1}$ means the inverse Laplace transformation and Im means the imaginary part of the vectors. Consequently, by substituting the Laplace-transformed I_1 of (9) into (10), the solution can be derived as

$$T=\frac{\dot{\theta}_sR_2M^2I_0^2}{z^2}-\left\{\frac{R_2M^2I_0^2}{lz}\ \sin\ (\dot{\theta}_st+\alpha)\right.$$
$$-\frac{L_{11}I_0}{l}[L_{22}I_0-l\ \mathrm{Re}\ (I_1|_{t=0})]\ \sin\ \dot{\theta}_st$$
$$\left.-L_{11}I_0\ \mathrm{Im}\ (I_1|_{t=0})\ \cos\ \dot{\theta}_st\right\}\ \exp\ (-R_2t/l) \quad (11)$$

where $z=[R_2^2+(\dot{\theta}_sl)^2]^{1/2}$, $\alpha=\tan^{-1}(\dot{\theta}_sl/R_2)$, and Re means the real part of the vectors. This equation represents the torque step response to the step change of $\dot{\theta}_s$ under a constant $|\psi_1|$. The first and second terms of (11) show steady-state and transient torque, respectively.

By differentiating (11) with respect to t, the rate of increasing torque at $t=0$ can be obtained.

$$\left.\frac{dT}{dt}\right|_{t=0}=\frac{L_{11}I_0}{l}\{[L_{22}I_0-l\ \mathrm{Re}\ (I_1|t=0)]\dot{\theta}s$$
$$-R_2\ \mathrm{Im}\ (I_1|t=0)\}. \quad (12)$$

Since the coefficient of $\dot{\theta}_s$ is always positive and large, the quick torque response can be attained by using as much $\dot{\theta}_s$ as possible. Fig. 2 shows some simulation results of the torque response to the step change of $\dot{\theta}_s$. The rate increase is approximately proportional to $\dot{\theta}_s$, but the torque has the maximum value at $\dot{\theta}_s=2\pi\cdot 15$ in the steady state.

III. Spacial Flux Vector Control by PWM Inverter

In the preceding section, an ideal power source with sinusoidal voltage and variable-frequency output was considered. In practice, a power source that has inherently stepwise voltage waveforms, such as a PWM inverter, should be considered. The instantaneous vectors of the PWM inverter are regarded as discrete values, and the analysis using the instantaneous vectors is suitable for investigating dynamic behavior of the machine.

Fig. 3 shows a schematic diagram of a PWM inverter drive system. In this figure the line-to-neutral voltage v_{1a}, v_{1b}, and v_{1c} are determined only by the inverter switching modes. Considering the combinations of status of switches S_a, S_b, and S_c, the inverter has eight conduction modes. By using switching functions S_a, S_b, and S_c, of which value is either 1 or 0, the primary voltage vector v_1 of (1) is represented as

$$v_1(S_a,\ S_b,\ S_c)=\sqrt{2/3}V[S_a+S_b\ \exp\ (j2\pi/3)$$
$$+S_c\ \exp\ (j4\pi/3)] \quad (13)$$

where V is the dc link voltage of the PWM inverter. According to the combination of the switching modes, the voltage vectors are specified for eight kinds of vectors, two of which are zero-voltage vectors $v_1(0, 0, 0)$ and $v_1(1, 1, 1)$, and the others are nonzero voltage vectors $v_1(0, 0, 1)$, $\cdots$, $v_1(1, 1, 0)$, as shown in Fig. 4 [6]–[8].

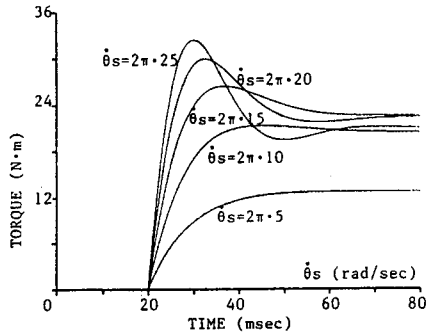

Fig. 2. Torque response for step change of $\dot{\theta}_s$.

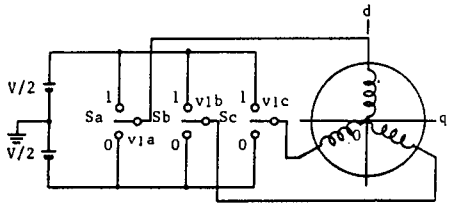

Fig. 3. Schematic diagram of PWM inverter.

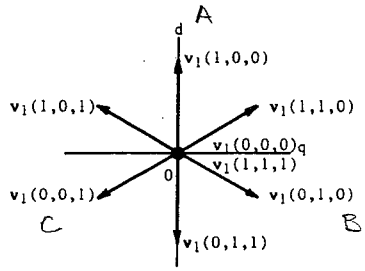

Fig. 4. Instantaneous voltage vectors.

Since the flux linkage vector is expressed by an integral of the voltage vector, substituting (6) into the stator equation in (4), the primary flux linkage vector ψ_1 is represented as a different style as follows

$$\psi_1 = \int (v_1 - R_1 i_1)\, dt. \tag{14}$$

During the switching intervals, each vector $v_1(0, 0, 0), \cdots, v_1(1, 1, 1)$ is constant so that substituting (13) into (14) gives

$$\psi_1 = \sqrt{2/3}V[S_a + S_b \exp(j2\pi/3) + S_c \exp(j4\pi/3)]t - R_1 \int i_1\, dt + \psi_1|_{t=0}. \tag{15}$$

Considering that the voltage drop of the winding is small, the trajectory of ψ_1 moves in the direction of the inverter output voltage vector [7]–[9]. When the output is one of the nonzero voltage vectors, ψ_1 moves at a constant velocity which is proportional to the output voltage. In the case of a zero voltage vector, the velocity is very small and considered to be approximately zero because of the small value of $R_1 i_1$. Therefore, by selecting these vectors appropriately, the trajectory of ψ_1 can follow up to the specified locus. For example, by selecting adequate voltage vectors, $|\psi_1|$ can be kept constant, as illustrated in Fig. 5, and the rotating velocity of ψ_1 can be controlled by changing the output ratio between zero vectors and the others.

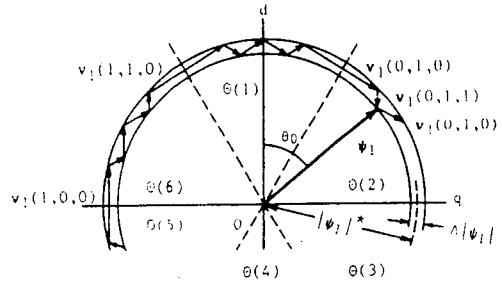

Fig. 5. Selection of voltage vectors for ψ_1.

Thus $\dot{\theta}_s$ and $|\psi_1|$ are greatly concerned with the dynamic torque and efficiency. If the amplitude and rotating velocity of ψ_1 can be changed freely, both desirable torque control and minimum-loss operation would be obtained at a time.

IV. Torque Control for Quick Response

Fig. 5 shows an example of constant $|\psi_1|$ control. The selection of $v_1(S_a, S_b, S_c)$ is made so that the error between $|\psi_1|$ and its command $|\psi_1|^*$ satisfies to be within the limits of $\Delta|\psi_1|$, i.e.,

$$|\psi_1|^* - \Delta|\psi_1|/2 \leqq |\psi_1| \leqq |\psi_1|^* + \Delta|\psi_1|/2. \tag{16}$$

The selection depends not only on the error of the amplitude, but also on the direction of ψ_1. As shown in Fig. 5, the inverter output voltage vectors change periodically by $\pi/3$ rad steps. Accordingly, to discriminate the direction, the d–q plane is divided into six regions as

$$(2N-3)\pi/6 \leqq \Theta(N) \leqq (2N-1)\pi/6 \tag{17}$$

where $N = 1, \cdots, 6$. For example, if ψ_1 is in the region of $\Theta(2)$, $v_1(0, 1, 0)$ and $v_1(0, 1, 1)$ can satisfy (16) for clockwise rotation. When $|\psi_1|$ reaches the upper limit of $|\psi_1|^* + \Delta|\psi_1|/2$, $v_1(0, 1, 1)$ must be selected. When $|\psi_1|$ reaches the lower limit of $|\psi_1|^* - \Delta|\psi_1|/2$, $v_1(0, 1, 0)$ must be selected. On the other hand, for counterclockwise rotation, $v_1(1, 0, 0)$ and $v_1(1, 0, 1)$ should be selected in $\Theta(2)$. Thus two-dimensional limit cycle control of ψ_1 makes possible a constant $|\psi_1|$ by selecting the appropriate voltage vectors.

According to (12), under constant $|\psi_1|$ control the rate of increasing torque is almost proportional to $\dot{\theta}_s$. Therefore, when T is small compared with its command T^*, it is necessary to increase T as fast as possible by applying the fastest $\dot{\theta}_0$. Accelerating vectors that possess the maximum $\dot{\theta}_0$ of clockwise direction can be uniquely selected by the regions $\Theta(N)$. When T reaches T^*, it is better to decrease T as slowly as possible for decreasing the inverter switching frequency. The slowest degenerative operation might be obtained by using zero voltage vectors. Fig. 6 shows torque control of this scheme for the clockwise operation. The selection of $v_1(S_a, S_b, S_c)$ is made so that the error of T satisfies to be within the limits of both ΔT and $\Delta|\psi_1|$, i.e.,

$$T^* - \Delta T \leqq T \leqq T^* \text{ when } \psi_1 \text{ rotates clockwise,}$$

$$T^* \leqq T \leqq T^* + \Delta T \text{ when } \psi_1 \text{ rotates counterclockwise.} \tag{18}$$

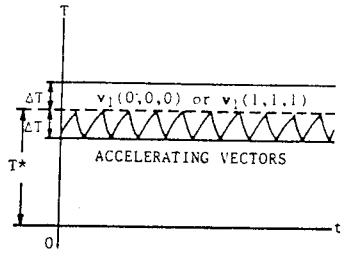

Fig. 6. Selection of voltage vectors for T.

Assuming that ψ_1 rotates clockwise, when T reaches T^*, a zero voltage vector is selected to stop ψ_1 and degenerate T. This corresponds to the case of $\dot{\theta}_s = -\dot{\theta}_m < 0$ in (12). On the other hand, when T reaches $T^* - \Delta T$, one of the accelerating vectors which rotates ψ_1 clockwise at maximum angular velocity is selected. For counterclockwise rotation, the zero and one of the accelerating voltage vectors that rotate ψ_1 counterclockwise with as much velocity are alternately selected to satisfy $T^* \leqq T \leqq T^* + \Delta T$.

As shown in Fig. 7, the status of the errors of $|\psi_1|$ and T can be detected and digitalized by simple two- and three-level hysteresis comparators. The contents of the optimum switching table, as stated before, is determined only by the errors and region $\Theta(N)$. Accordingly, accessing the table, in which the inverter output voltage vectors are listed by the comparator outputs and $\Theta(N)$ signals, the optimum switching pattern desirable for drive can be directly obtained. In this figure, ϕ and τ are digitalized outputs of the errors, and the signals of the $\Theta(N)$ are generated by comparing d- and q-axis components of the flux linkage vector with its amplitude. The switching table is referred by the outputs of the comparators ϕ, τ, and $\Theta(N)$. A combination of them defines only an inverter output voltage vector $v_1(S_a, S_b, S_c)$.

V. Experimental System and Results

Fig. 8 shows a configuration of the proposed system. In this system, the d- and q-axis variables are used for convenience instead of the instantaneous vectors. So the three-to-two phase transformations for the primary voltage and current are given by

$$v_1 = v_{1d} + jv_{1q}$$

$$= \sqrt{2/3}[v_{1a} - v_{1b}/2 - v_{1c}/2 + j(\sqrt{3}v_{1b}/2 - \sqrt{3}v_{1c}/2)],$$

$$i_1 = i_{1d} + ji_{1q}$$

$$= \sqrt{2/3}[i_{1a} - i_{1b}/2 - i_{1c}/2 + j(\sqrt{3}i_{1b}/2 - \sqrt{3}i_{1c}/2)]. \quad (19)$$

Substituting (19) into (14), the components of the primary flux linkage vector are expressed as

$$\psi_1 = \psi_{1d} + j\psi_{1q}$$

$$= \int (v_{1d} - R_1 i_{1d})\, dt + j \int (v_{1q} - R_1 i_{1q})\, dt. \quad (20)$$

The d- and q-axis components of ψ_1 can be easily calculated by using integrators as shown in (20). The electromagnetic

$\phi,\tau,\Theta(N)$		$\Theta(1)$	$\Theta(2)$	$\Theta(3)$	$\Theta(4)$	$\Theta(5)$	$\Theta(6)$
$\phi=1$	$\tau=1$	$v_1(1,1,0)$	$v_1(0,1,0)$	$v_1(0,1,1)$	$v_1(0,0,1)$	$v_1(1,0,1)$	$v_1(1,0,0)$
	$\tau=0$	$v_1(1,1,1)$	$v_1(0,0,0)$	$v_1(1,1,1)$	$v_1(0,0,0)$	$v_1(1,1,1)$	$v_1(0,0,0)$
	$\tau=-1$	$v_1(1,0,1)$	$v_1(1,0,0)$	$v_1(1,1,0)$	$v_1(0,1,0)$	$v_1(0,1,1)$	$v_1(0,0,1)$
$\phi=0$	$\tau=1$	$v_1(0,1,0)$	$v_1(0,1,1)$	$v_1(0,0,1)$	$v_1(1,0,1)$	$v_1(1,0,0)$	$v_1(1,1,0)$
	$\tau=0$	$v_1(0,0,0)$	$v_1(1,1,1)$	$v_1(0,0,0)$	$v_1(1,1,1)$	$v_1(0,0,0)$	$v_1(1,1,1)$
	$\tau=-1$	$v_1(0,0,1)$	$v_1(1,0,1)$	$v_1(1,0,0)$	$v_1(1,1,0)$	$v_1(0,1,0)$	$v_1(0,1,1)$

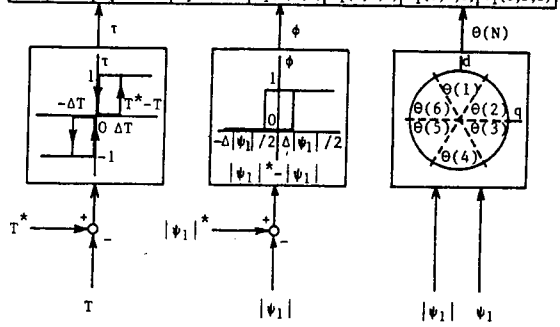

Fig. 7. Optimum switching table and comparators.

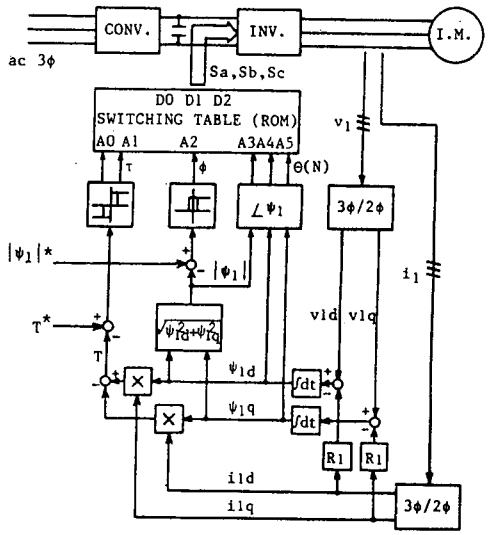

Fig. 8. Block diagram of proposed system.

torque in (5) is rewritten as

$$T = \psi_{1d} i_{1q} - \psi_{1q} i_{1d}. \quad (21)$$

The equation shows that the torque can be estimated by only the primary variables. Then the errors of the amplitude of the flux and torque need to be digitalized by two- and three-level hysteresis comparators, respectively, and the digitalized direction of ψ_1, $\Theta(N)$, is determined by comparing ψ_{1d} and ψ_{1q} with $\pm\sqrt{3}/2|\psi_1|$ or $\pm 1/2|\psi_1|$ using some comparators and logic circuits. The optimum switching table is referred by the digital signals, i.e., one bit of ϕ, two bits of τ, and three bits of $\Theta(N)$. Thus the optimum voltage vector $v_1(S_a, S_b, S_c)$ can be obtained directly by accessing the address of the ROM, of which memory size is only 64 bytes. If an analog-to-digital (A/D) converter were employed instead of the comparators, even better performance and more precise control would be expected. The outputs of the ROM are used directly to drive the power transistors after isolation by photocouplers.

The control circuit can be simplified because the scheme needs neither the secondary variables and constants of the machine nor the coordinate transformation using a position

sensor, whereas integrators cause some drift and operation errors at low-velocity regions. But the effect is very small above 2 Hz, so the compensation for flux calculation is not always necessary at normal operation. For extremely low velocity operation, another estimation of the flux may be necessary.

Experiments were carried out to verify the feasibility of the proposed scheme using a 1.5-kW three-phase induction motor. Fig. 9(a) shows a locus of the primary flux linkage in the steady state. $|\psi_1|$ is controlled to be approximately constant, and several bright spots show the points where ψ_1 halts. Since flux ripples are relatively small and minor loops are not observed in this locus, harmonic losses and acoustic noise of the machine may be effectively decreased [9]. Fig. 9(b) shows a velocity step response obtained in the experiment. The response time for the velocity difference of 500 r/min is about 8 ms. Even in the transient operation, $|\psi_1|$ can be kept constant, owing to the limit cycle control, except for saturation of the inverter. The harmonic components of the electromagnetic torque are also restricted within the hysteresis bands. The switching frequency of the comparators is identical with that of the PWM inverter. Hence, using the proposed control the inverter switching frequency can be reduced under the same condition of torque and flux ripple in comparison with the other schemes. Since the ripples have close relation to the acoustic noise and harmonic losses, the proposed scheme will make possible the decrease of not only the inverter switching frequency, but also the other harmful components.

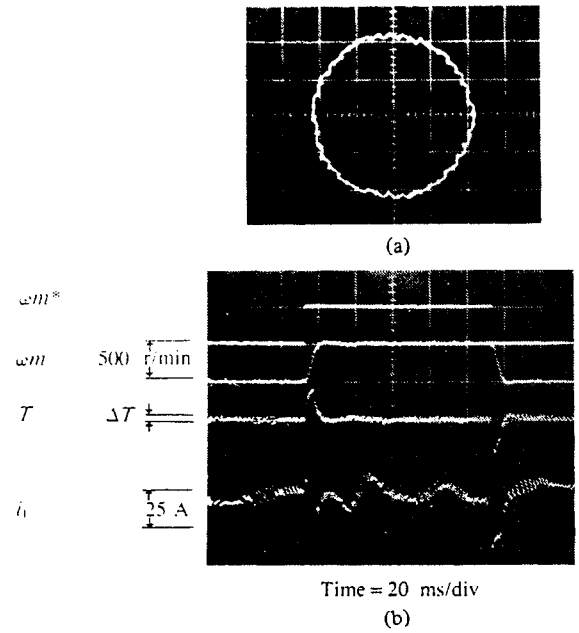

Fig. 9. Experimental results. (a) Locus of ψ_1 at 600 r/min. (b) Velocity step response.

VI. Comparison with Field-Oriented Control

Assuming field-oriented control employing an instantaneous current-controlled inverter by hysteresis comparators, and the same inverter switching frequency and dc link voltage, the comparison between field-oriented and the proposed control is performed.

Fig. 10(a) and (b) show simulation results of the torque step responses from 5–15 N·m. As shown in this figure, the flux ripples of both schemes are almost same, whereas the torque ripple of this scheme is about half the conventional in the steady state.

It has been said that the field-oriented controller can achieve the torque response instantaneously. But this can be said only when the inverter can achieve instantaneous current control sufficiently. In other words, when the inverter output voltage is limited, the instantaneous response would not be assured. In the proposed system, the optimum voltage vector can be selected to obtain as fast torque response as possible at every instant. Therefore the response when the inverter saturates bears comparison with that of field-oriented control. Moreover, owing to the effective switching operation, the reduction of the inverter switching frequency is remarkable, especially in the low-velocity operation.

Representing the effect of the rotor resistance variations on the response, (12) clearly shows that the increase of R_2 causes deterioration of the response. Fig. 11 shows that the small deterioration of the response time is observed as R_2 increases. In the practical case, however, the deviations of R_2 from 0.5 R_2 to 1.5 R_2 would scarcely cause serious problems. Thus torque limit cycle control employed in this scheme is very effective for designing a robust system. On the other hand, the deviations of the stator resistance R_1 in calculating ψ_1 using (14) at low velocities causes some errors. Therefore implementation of a compensator for the flux calculation is necessary.

VII. Compensation for Flux Calculation

(14) indicates that the primary flux linkage vector ψ_1 can be calculated from only the primary variables, which are observable and measured with simple circuits. Some problems, however, would arise from the integral operation at extremely low velocities. The reason for this is that the operation of integrators can not be done perfectly at zero velocity because of no induced electromotive force in the motor, so that control of ψ_1 might be unstable when R_1 deviates from the correct value. These problems are negligible at relatively high velocities such as above 2 Hz. But another calculation of ψ_1 must be employed below 2 Hz.

Transforming (4) with respect to an α–β frame synchronously rotating with the rotor, the result can be written as

$$\begin{bmatrix} v_1' \\ 0 \end{bmatrix} = \begin{bmatrix} R_1 + (p + j\dot{\theta}_m)L_{11} & (p + j\dot{\theta}_m)M \\ pM & R_2 + pL_{22} \end{bmatrix} \begin{bmatrix} i_1' \\ i_2' \end{bmatrix}. \tag{22}$$

and the flux linkage vector in the α–β frame is

$$\psi_1' = L_{11} i_1' + M i_2'. \tag{23}$$

Substituting i_2' from the rotor equation into (23), ψ_1' can be rewritten with respect to i_1' as follows

$$\psi_1' = L_{11} \frac{1 + p(l/R_2)}{1 + p(L_{22}/R_2)} i_1'. \tag{24}$$

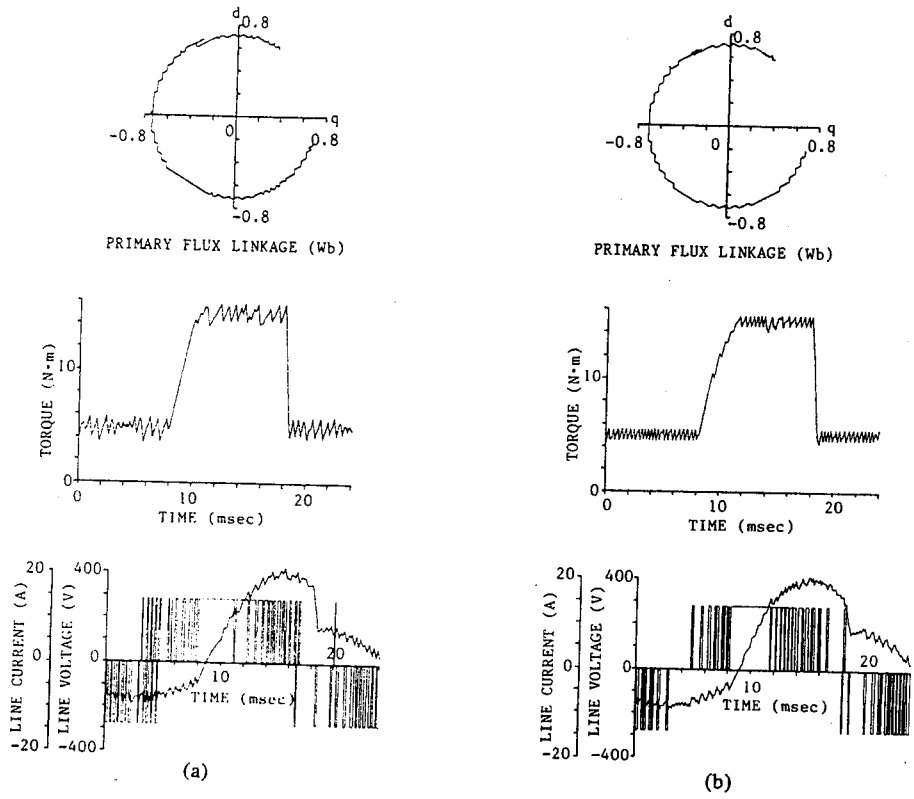

Fig. 10. Simulation results for comparison between schemes. (a) Field-oriented control. (b) Proposed control. (Induction motor parameters: $R_1 = 0.5\ \Omega$; $R_2 = 1.0\ \Omega$; $L_{11} = 0.105$ H; $L_{22} = 0.105$ H; $M = 0.1$ H; number of poles = 2; $\dot{\theta}_m = 188.5$ rad/s; 1800 r/min; $V = 280$ V; switching frequency = 2.5 kHz.)

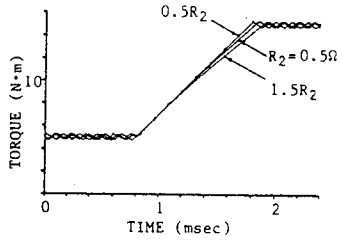

Fig. 11. Torque step response for variations of R_2.

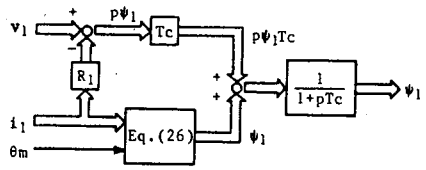

Fig. 12. Improved flux estimator.

Equations describing the coordinate transformation are

$$\psi_1 = \psi_1' \exp(j\theta_m),\quad i_1' = i_1 \exp(-j\theta_m). \tag{25}$$

Then, substituting (25) into (24) gives

$$\psi_1 = \left\{ L_{11} \frac{1 + p(l/R_2)}{1 + p(L_{22}/R_2)} [i_1 \exp(-j\theta_m)] \right\} \exp(j\theta_m). \tag{26}$$

Hence, ψ_1 can be calculated from i_1 and θ_m, even at low velocities, but variations of R_2 affect this calculation [6].

Accordingly, to calculate the flux precisely, it is better to employ (14) than (26) at relatively high velocities. At low velocities, such as below 2 Hz, (26) is better to the contrary. Fig. 12 shows an improved flux estimator circuit composed of a simple lag network. The input of the network is Tc $p\psi_1$ + ψ_1; therefore the output is equal to ψ_1. In this figure the time constant Tc must be specified so as to minimize automatically the calculation error when the flux equation changes from (14) to (26). In the case of the low-velocity operation, i.e., ω Tc $\ll$ 1, the network behaves as a circuit of unity transfer function. Thus its output becomes almost ψ_1 of (26) because of the small value of $v_1 - R_1 i_1$ in (14). In the high-velocity operation, since 1 $\ll \omega$ Tc, the transfer function is approximately shown as $1/s$, which corresponds to that of the integrator. Hence these actions are switched over smoothly around the frequency of 1/Tc.

Fig. 13(a) shows the trajectory of ψ_1 at 1 r/min when the stator resistance varied by +20 percent. The trajectory is shifted and, as a result, ψ_1 would be saturated. Fig. 13(b) shows the compensated result. As can be seen from this figure, the shifting is fully compensated.

VIII. Flux Control for Efficiency Improvement

Torque control is skillfully obtained by controlling the instantaneous slip angular frequency, whereas the improvement of the efficiency can be achieved by controlling the amplitude of ψ_1 like a field-weakening operation. In the case

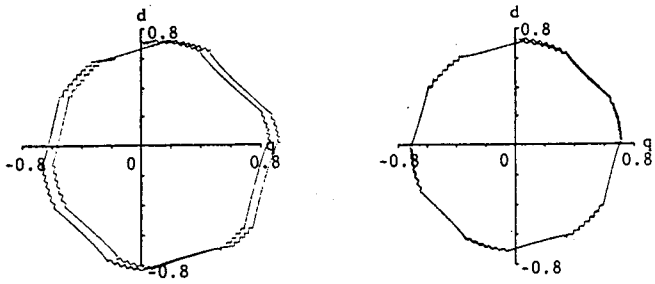

Fig. 13. Locus of ψ_1. (a) Case of 1.2 R_1. (b) Compensated result.

of frequent changes of the torque command, it is necessary to keep the amplitude at maximum. Under the field-weakened state, the sufficient torque or quick torque response would not be expected because of the slow response of the flux increase. On the other hand, in the steady-state operation, especially at light loads, the maximum efficiency can be obtained at a low flux level. Therefore, in order to obtain the maximum efficiency the flux level is adjusted automatically in accordance with the torque command.

The total loss of the induction motor is expressed by

$$P \text{ loss } = R_1 I_1^2 + R_2' I_2'^2 + R_i I_0^2 \tag{27}$$

where

R_2'	R_2 referred to the stator,
R_i	equivalent resistance of the iron loss,
I_1 and I_2'	rms values of I_1 and I_2 referred to the stator, respectively.

The equation can be rewritten with respect to I_2' and I_0 as

$$P \text{ loss} = (R_1 + R_2')I_2'^2 + (R_1 + R_i)I_0^2 + 2R_1 I_0 I_2' \cos \beta \tag{28}$$

where the trajectory of I_2' is on the circle C as shown in Fig. 14. β is the phase difference between I_0 and I_2'. The electromagnetic torque of (10) can also be rewritten using β:

$$T = L_{11} I_0 I_2' \sin \beta. \tag{29}$$

Since the voltage across the leakage reactance $\omega(L_{11}/M)^2 l I_2'$ is equal to $\omega L_{11} I_0 \cos \beta$, the following relation can be obtained:

$$I_2' = \frac{L_{11}}{(L_{11}/M)^2 l} I_0 \cos \beta. \tag{30}$$

Substituting (30) into (28) and (29) gives

$$P \text{ loss} = \frac{2(L_{11}/M)^2 lT}{L_{11}^2} \left(\frac{A \cos^2 \beta + B}{\sin \beta} \right) \tag{31}$$

where

$$A = \frac{L_{11}}{(L_{11}/M)^2 l} [L_{11}(R_1 + R_2')/(L_{11}/M)^2 l + 2R_1]$$

$$B = R_1 + R_i.$$

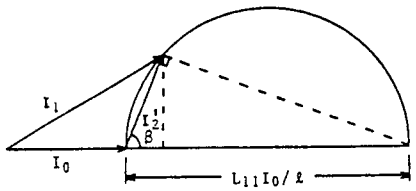

Fig. 14. Circular diagram.

The total loss of (31) has the minimum value at $\beta = \tan^{-1} \sqrt{(A + B)/B}$. Substituting $\beta = \tan^{-1} \sqrt{(A + B)/B}$ into (29) and (30), the following solution is derived:

$$T = \frac{\sqrt{AB + B^2}}{(L_{11}/M)^2 l (A + 2B)} |\psi_1|^2. \tag{32}$$

The coefficient in (32) is regarded as a function of primary angular frequency ω_0 because B includes R_i.

Fig. 15 shows a block diagram of the efficiency controller. The flux command $|\psi_1|^*$ is calculated from the torque command T^* and ω_0 based on (32). In this figure a nonlinear active filter is composed of an integrator with a diode. It behaves like a peak holder when the torque command T^* changes frequently. The integrator output voltage increases as fast as possible because of the small charging time constant. Once the voltage settles to a certain value, it decreases very slowly because the discharging time constant is very large. These time constants are specified appropriately according to the frequency of the torque command change.

Fig. 16(a) and (b) show examples of improved results of the efficiency and acoustic noise, respectively. When the amplitude of ψ_1 is 33 percent of the maximum value, no load loss can be improved less than 70 W, and the acoustic noise level is also decreased by 10–15 dB.

IX. Conclusion

Novel induction motor control optimizing both torque response and efficiency is proposed. The control is quite different from the usual field-oriented control because it depends on the concept of the instantaneous slip frequency control, in spite of the electromagnetic force. In other words, the former is to Arago's law as the latter is to Fleming's law.

Through the experimental and simulation techniques, the validity of the proposed theory can be proven. The main results obtained in this paper are as follows.

1) In the transient state, the highest torque response can be obtained by selecting the fastest accelerating voltage vector to produce the maximum slip frequency.
2) In steady state, by selecting the accelerating vector and the zero voltage vector alternately, the torque can be maintained constant with small switching frequency by the hysteresis comparator of torque. Accordingly, the harmonic losses and the acoustic noise level of the motor can be reduced.
3) The amplitude of the primary flux is also controlled to attain the maximum efficiency in steady-state operation. The flux level can be automatically adjusted to get the

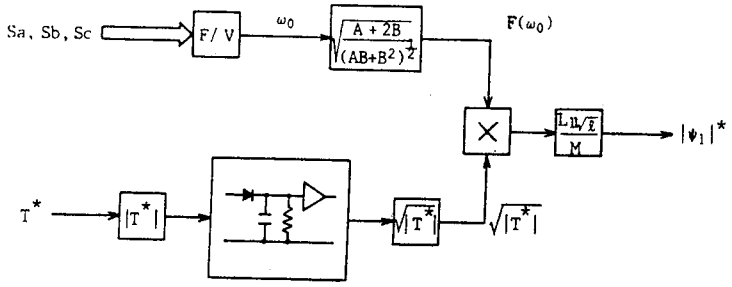

Fig. 15. Block diagram of efficiency controller.

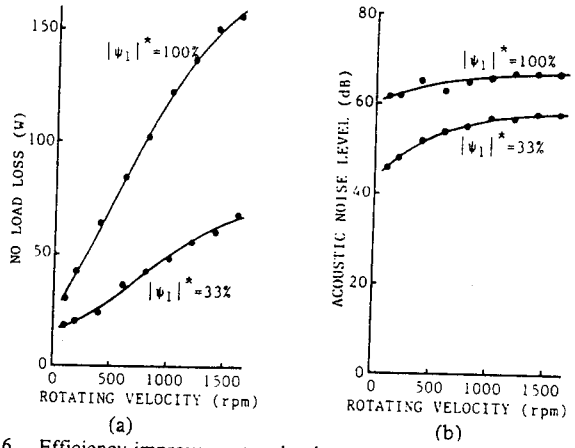

Fig. 16. Efficiency improvement and noise reduction. (a) No load loss. (b) Acoustic noise level.

optimum efficiency in the steady state and the highest torque response in the transient state at the same time by using a nonlinear active filter.

4) At extremely low frequency operation, the proposed control circuit makes some drift, but can be compensated easily and automatically to minimize the effect of the variation of the machine constants.

The proposed scheme is found to be very promising and valuable as compared to field-oriented control. All results show that the scheme is superior in every respect to field-oriented control.

Acknowledgment

The authors wish to express their appreciation to the Power Electronics Laboratory members of The Technological University of Nagaoka.

References

[1] A. Nabae, K. Otsuka, H. Uchino, and R. Kurosawa, "An approach to flux control of induction motors operated with variable-frequency power supply," *IEEE Trans. Ind. Appl.*, vol. IA-16, pp. 342–350, May/June 1980.

[2] L. J. Garces, "Parameter adaption for the speed controlled static ac drive with a squirrel-cage induction motor," *IEEE Trans. Ind. Appl.*, vol. IA-16, pp. 173–178, Mar./Apr. 1980.

[3] K. B. Nordin, D. W. Novotny, and D. S. Zinger, "The influence of motor parameter deviations in feedforward field orientation drive systems," in *Conf. Rec. 1984 Ann. Meet. IEEE Ind. Appl. Soc.*, pp. 525–531.

[4] T. Matsuo and T. A. Lipo, "A rotor parameter identification scheme for vector controlled induction motor drives," in *Conf. Rec. 1984 Ann. Meet. IEEE Ind. Appl. Soc.*, pp. 538–545.

[5] T. Noguchi and I. Takahashi, "Quick torque response control of an induction motor based on a new concept," presented at IEEJ Tech. Meet. on Rotating Machine RM84-76, pp. 61–70, Sep. 1984.

[6] I. Racz, "Dynamic behavior of inverter controlled induction motors," in *Conf. Rec. 1965 IFAC*, pp. 4B.1–4B.7.

[7] K. R. Jardan, S. B. Dewan, and G. R. Slemon, "General analysis of three-phase inverters," *IEEE Trans. Ind. Gen. Appl.*, vol. IGA-5, pp. 672–679, Nov./Dec. 1969.

[8] K. R. Jardan, "Modes of operation of three-phase inverters," *IEEE Trans. Ind. Gen. Appl.*, vol. IGA-5, pp. 680–685, Nov./Dec. 1969.

[9] Y. Murai and Y. Tsunehiro, "Improved PWM method for induction motor drive inverters," in *Conf. Rec. 1983 IPEC*, pp. 407–417.

Isao Takahashi (M'81) was born in Japan on March 10, 1942. He received the B.S. degree in 1966 and the Ph.D. degree in 1971, both in electrical engineering, from the Tokyo Institute of Technology.

He was an Assistant Professor at the Tokyo Institute of Technology from 1971 to 1975 and an Associate Professor at Utsunomiya University from 1975 to 1978. He was a Visiting Associate Professor at the University of Wisconsin in 1982. Since 1978, he has been an Associate Professor of electrical and electronics system engineering at the Technological University of Nagaoka, Japan. His current research interests are in high-power optimum control, especially motor drives, power active filters, flywheel energy storage systems, optimum control of the PWM inverter, high-frequency power systems, and power system control of an atomic fusion reactor.

Dr. Takahashi is a member of IEEE.

Toshihiko Noguchi was born in Japan on October 23, 1959. He received the M.S. degree in electrical and electronics system engineering from the Technological University of Nagaoka in 1986.

In 1982, he joined the Toshiba Corporation, Mie Prefecture, Japan, and his current works are on the static power converter and motor control.